

Determination of Domain Wall Velocity and Nucleation Time by Switching Dynamics Studies of Ferroelectric Hafnium Zirconium Oxide

Xiao Lyu¹, Pragma R. Shrestha^{2,3}, Mengwei Si¹, Panni Wang⁴, Junkang Li¹, Kin P. Cheung³, Shimeng Yu⁴ and Peide D. Ye^{1,*}

¹School of Electrical and Computer Engineering, Purdue University, West Lafayette, USA. *Email: yep@purdue.edu

²Theiss Research, La Jolla, USA. ³National Institute of Standards and Technology, Gaithersburg, USA.

⁴School of Electrical and Computer Engineering, Georgia Institute of Technology, Atlanta, USA.

Abstract

In this work, we present the first experimental determination of nucleation time and domain wall (DW) velocity by studying switching dynamics of ferroelectric (FE) hafnium zirconium oxide (HZO). Experimental data and simulation results were used to quantitatively study the switching dynamics. The switch speed is degraded in high aspect ratio devices due to the longer DW propagation time or with dielectric interfacial layer due to the required additional tunneling and trapping time by the leakage current assist switch mechanism.

Introduction

As a CMOS-compatible material, its scalability, high energy efficiency and remarkable reliability performance [1, 2] make FE HfO₂ the promising material for device applications. Operational speed [3-11] is a key challenge for commercialization of FE HfO₂ based devices. While sub-ns switching was demonstrated [3-5, 11], how much faster can it go is a key question remains to be answered. Parasitic effects have prevented the experimental investigation of fundamental parameters such as nucleation time t_N and domain wall (DW) propagation velocity v_{DW} until now. FE HZO capacitors with various shapes and interfacial layer thicknesses were studied with transient current measurements. The t_N and v_{DW} are determined experimentally for the first time in FE HZO according to the NLS model. We found that devices with higher aspect ratio (length/width in 2D rectangular shape) is found to switch slower statistically due to longer DW propagation time in length. In addition, interfacial layer causes a minor increase on the overall switching time due to the required tunneling and trapping time of the leakage current through the DE layer.

Experiments

The fabrication process flow and device structure are as described in Fig. 1. Tungsten was used as electrodes to promote the crystallization of FE phase while keeping a small series resistance. The growth of HZO was by atomic layer deposition (ALD) at 200 °C [3]. In order to understand the FE switching of FE/DE gate stack, part of the sample set was deposited with Al₂O₃ interfacial layers. Rectangular crossbars were designed to have different aspect ratio and area. All the samples show strong ferroelectricity as illustrated in Fig. 2. The circuit diagram of the ultrafast pulse measurement setup is illustrated in Fig. 3 and established methodology can be found in [3, 5].

Results and Discussion

A representative PUND transient current measurement of these devices is shown in Fig. 4. The transient current responses of the switching pulse and non-switching pulse are measured. Fig. 5 shows the transient current I_{pulse1} , I_{pulse2} and the extracted net switching current I_{FE} in the same plot as an intuitive example. The switching current is extracted by the subtraction of I_{pulse1} and I_{pulse2} . The time response of ferroelectric polarization switching charge can be calculated by integrating the net switching current. Fig. 6 shows the FE polarization switching charge versus time with the theoretical model fitting by $P = P_s(1 - \exp(-(\frac{t}{\tau_0})^2))$, in which the τ_0 parameter is a characteristic switching time constant [9, 12].

The measured switching time constant dataset of single crossbar devices on the 15 nm HZO sample is shown in Fig. 11. The crossbars are divided into 3 groups with the identical area and different aspect ratios. The switching time τ_0 increases with higher aspect ratio in every group, containing the DW propagation information [13]. The offset values at aspect ratio of 1 for the 3 different area groups give the area dependent t_N information. If we

assume simply $t_0 = t_N + L/v_{DW}$, Fig. 7 can be re-plotted as Fig. 8 after subtracting the different t_N (total areas). L is the length of the long edge. Fig. 8 presents the first main conclusion of this work that v_{DW} of HZO is 4.1×10^4 m/s, similar to Pb(Nb_{0.04}Zr_{0.28}Ti_{0.68})O₃ [14]. Fig. 9 presents a new plot based on Fig. 7 with the offset values of t_0 versus the characteristic length. After fitting the three available data, we can obtain the second main conclusion of this work that geometry independent t_N (t_{N0}) is 560 ps in this set of devices. Note that these obtained values are only determined from this set of devices with the structures and material growth conditions. The obtained t_{N0} contains the limitation of the electric pulse rise time and parasitic RC constants of the device and measurement setup. The intrinsic t_N in HZO must be shorter and dependent on the thickness of HZO. Fig. 10 illustrates the physical mechanism underpinning this work, implying that the methodology can be applied to other FE films. Fig. 11 highlights the impact of aspect ratio on the FE switching. When the device area increases while keeping one edge of the device unchanged, the switching time constant has notable difference between the high and low aspect ratio case. The error bars in the plot suggest that statistically high aspect ratio devices have larger device-to-device variation. This suggests that the long edge of the device limits its switching speed by v_{DW} . Since the location of the first flipped domain is randomly distributed, a higher aspect ratio naturally leads to a larger speed variation.

Simulation study based on the time-dependent Landau-Ginzburg framework (TDLG) [15, 16] was also applied to give more insight into the impact of device geometry on the FE switching process. Because of the domain-to-domain variation, some domains have low microscopic coercive field and are easily flipped. The normalized coercive-field distribution map was generated following Gaussian distribution (Fig. 12). The multi-domain switching dynamics was simulated by calculating the polarization response distribution over the sample based on the coercive field map. The change of polarization distribution over time of a square shaped device is shown in Fig. 13. In comparison, the polarization switching process is less efficient in another device with an aspect ratio of 25 (Fig. 14). The simulation P-t curves of devices with various shape and same area are plotted in Fig. 15.

To determine the impact of interfacial layer, the speed of FE/DE crossbar devices are measured in comparison with FE HZO devices of the same geometry, as shown in Fig. 16. The switching time constants in Fig. 17 suggest that only minor speed degradation was caused by the Al₂O₃ layer. The mechanism of the extra switching time is likely from the tunneling and trapping process in the leakage-assist switching mechanism [17] as depicted in the inset of Fig. 20.

Conclusions

Nucleation time and domain wall velocity in HZO are determined for the first time by experimental study with switch dynamics. Experiments are in accordance with the NLS model and TDLG simulation results. The aluminum oxide interfacial layer is found to slow down the switching speed to a limited extent. The work was supported by DARPA/SRC JUMP ASCENT Center.

Reference [1] K. Ni *et al.*, *IEEE TED*, vol. 65, p. 2461, 2018. [2] N. Gong *et al.*, *IEEE EDL*, vol. 37, p. 1123, 2016. [3] X. Lyu *et al.*, *IEEE IEDM*, p.342, 2019. [4] W. Chung *et al.*, *IEEE Symposium on VLSI*, p. T89, 2018. [5] M. Si *et al.*, *Appl. Phys. Lett.* vol. 115, p. 072107, 2019. [6] E. Yurehuk *et al.*, *IEEE TED*, vol. 61, p. 3699, 2014. [7] H. K. Yoo *et al.*, *IEEE IEDM*, p. 481, 2017. [8] S. Dunkel *et al.*, *IEEE IEDM*, p. 488, 2017. [9] C. Alessandri *et al.*, *IEEE EDL*, vol. 39, pp. 1780-1783, 2018. [10] K. Karda *et al.*, *IEEE EDL*, vol. 37, p. 801, 2016. [11] X. Lyu *et al.*, *IEEE SNW*, p. 7, 2020. [12] J. Y. Jo *et al.*, *Phys. Rev. Lett.* vol. 99, p. 267602, 2007. [13] D.-H. Choe *et al.*, *Materials Today*, vol. 50, p. 8, 2021. [14] J. Li *et al.*, *Appl. Phys. Lett.* vol. 84, p. 1174, 2004. [15] A. K. Saha *et al.*, *Appl. Phys. Lett.* vol. 114, p. 202903, 2019. [16] P. Wang *et al.*, *IEEE TED*, vol. 67, p. 3598, 2020. [17] M. Si *et al.*, *ACS Applied Electronic Materials*, p. 745, 2019.

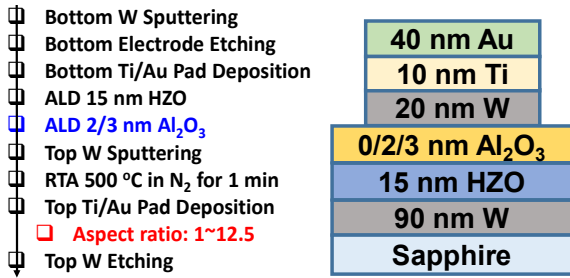


Fig. 1. Device fabrication process flow and cross sectional diagram for W/HZO/W crossbar devices.

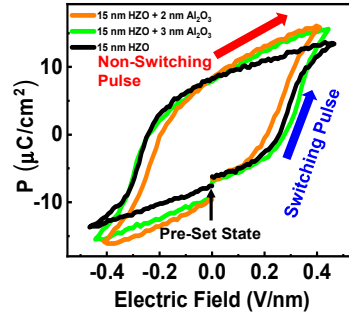


Fig. 2. P-E loops of single crossbar devices with oxide layer structures.

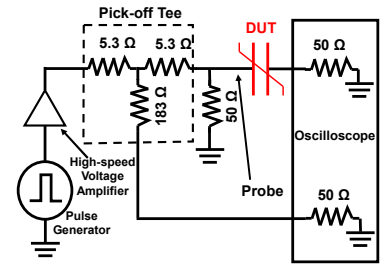


Fig. 3. Circuit diagram of the ultrafast pulse measurement setup.

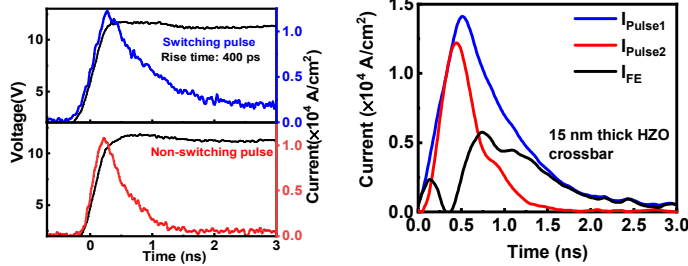


Fig. 4. Ultrafast pulse input and the corresponding current response of the switching (upper) and non-switching (lower) pulse.

Fig. 5. Measured transient currents and the extracted switching current of a 15 nm thick HZO crossbar device.

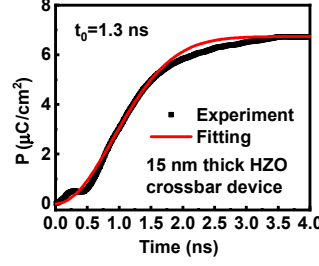


Fig. 6. Transient switched polarization charge density from experiment and theoretical model of a 15 nm thick HZO crossbar.

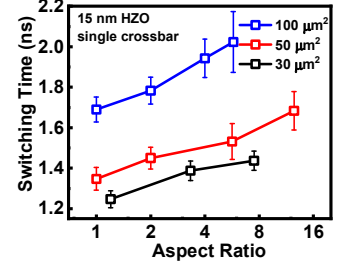


Fig. 7. The switching time versus device aspect ratio of various groups of devices with same area.

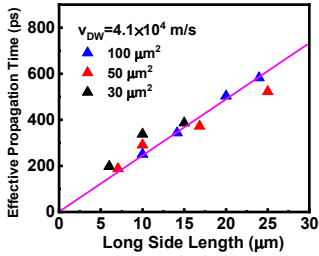


Fig. 8. Effective domain wall propagation time of various devices versus the long side length and the extracted DW velocity.

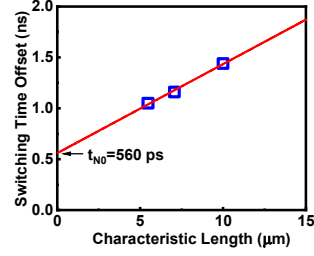


Fig. 9. Extraction of geometry independent nucleation time in 15 nm FE HZO capacitors. The characteristic length is defined as the square-root of the device area.

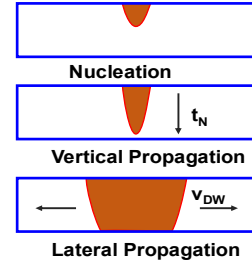


Fig. 10. Schematic of FE HZO thin film switch mechanism consisting of nucleation and domain wall propagation process.

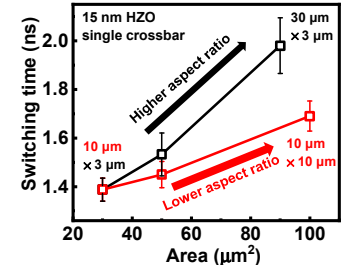


Fig. 11. Comparison of switching time increase with larger area and rising aspect ratio and reducing aspect ratio respectively.

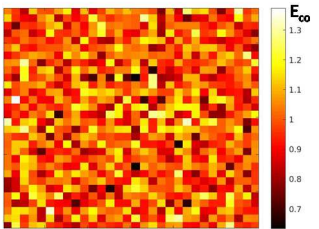


Fig. 12. Normalized coercive field distribution map generated by random Gaussian distribution.

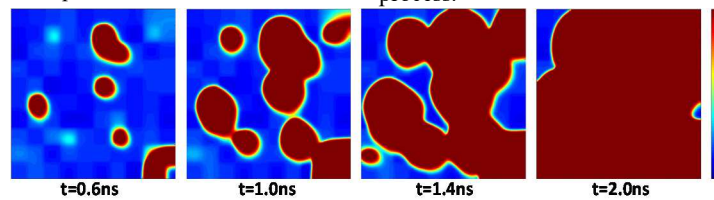


Fig. 13. The change of polarization distribution map over time of a square shaped device by phase-field model simulation based on TDLG.

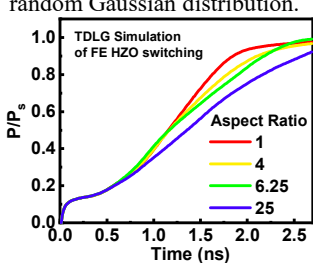


Fig. 15. Simulated transient polarization switching current of HZO capacitors with different aspect ratios.

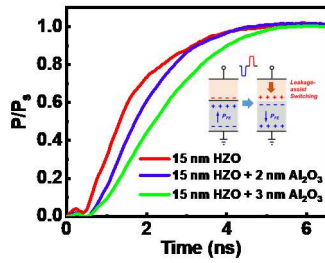


Fig. 16. Transient polarization charge density of devices with different dielectric layer thickness. The inset is a diagram of the leakage-assist switch mechanism in FE/DE oxide stack.

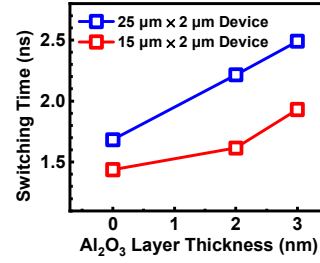


Fig. 17. Impact of additional Al₂O₃ dielectric layer on the 15 nm FE HZO device switching speed.

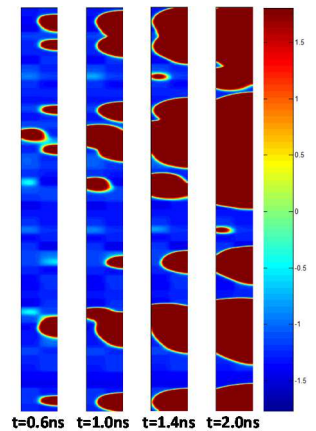


Fig. 14. The change of polarization distribution map over time of a device with an aspect ratio of 25 by TDLG simulation. The distribution map images are stretched for a better visual effect.